MAKARA, TEKNOLOGI, VOL. 14, NO. 2, NOVEMBER 2010: 53-60

DYE SENSITIZED SOLAR CELL WITH CONVENTIONALLY ANNEALED AND POST-HYDROTHERMALLY TREATED NANOCRYSTALLINE SEMICONDUCTOR OXIDE TiO_2 DERIVED FROM SOL-GEL PROCESS

Akhmad Herman Yuwono*), Badrul Munir, Alfian Ferdiansyah,
Arif Rahman, and Wulandari Handini

Department of Metallurgy and Materials Engineering, Faculty of Engineering, University of Indonesia,
Depok 16424, Indonesia

*)E-mail: ahyuwono@metal.ui.ac.id

Abstract

Dye-sensitized solar cell (DSSC) is one of the very promising alternative renewable energy sources to anticipate the declination in the fossil fuel reserves in the next few decades and to make use of the abundance of intensive sunlight energy in tropical countries like Indonesia. In the present study, TiO_2 nanoparticles of different nanocrystallinity was synthesized via sol−gel process with various water to inorganic precursor ratio (R_w) of 0.85, 2.00 and 3.50 upon sol preparation, followed with subsequent drying, conventional annealing and post-hydrothermal treatments. The resulting nanoparticles were integrated into the DSSC prototype and sensitized with an organic dye made of the extract of red onion. The basic performance of the fabricated DSSC has been examined and correlated to the crystallite size and band gap energy of TiO_2 nanoparticles. It was found that post-hydrothermally treated TiO_2 nanoparticles derived from sol of 2.00 R_w, with the most enhanced nanocrystalline size of 12.46 nm and the lowest band gap energy of 3.48 eV, showed the highest open circuit voltage (V_{oc}) of 69.33 mV.

Keywords: dye sensitized solar cell, hydrolysis ratio, post-hydrothermal, sol-gel, TiO_2

1. Introduction

There is no doubt that in the last few years the whole world has been facing a very critical problem for the sustainability of human being due to the declination of the fossil fuel reserves which is still being used as the main energy source in most of the countries. It is predicted that the oil supply in Indonesia is only sufficient for the next 18 years, although other energy sources such as gas and coal would still be available until the next 61 and 147 years, respectively [1]. At the same time, the increase of carbon emission from industries, houses and passenger cars has been polluting the air which caused green-house effect leading to the global warming. Therefore, with the declination of the fossil fuel reserves and the improved awareness of the environmental issues, the search for sustainable energy becomes more important and unavoidable. The viable alternative to hydrocarbons has taken many paths including nuclear, wind power, geothermal and solar. Among others, solar cell, as a photovoltaic device which generates electricity directly from sunlight, provides an attractive form of limitless alternative energy. Currently, silicon solar cell have the highest solar energy conversion of around 24%, however the efficiency is offset by the high cost of production [2]. Therefore, research into cheaper and more efficient solar cells has been underway for several decades. In this context, dye-sensitized solar cells (DSSC) based on nanocrystalline inorganic oxide such as TiO_2, ZnO and SnO_2 have attracted much attention since their first description in the beginning of the 1990s by Grätzel and O'Reagan [3]. Nowadays, overall efficiencies of 11% have been reported for DSSC using liquid electrolyte [4]. In a typical DSSC, the high surface area nanoparticle oxide layer is sensitized with a charge transfer ruthenium complex dye, which absorbs light in the visible range of the solar spectrum. Energy conversion is obtained by injection of the electrons from the photo-excited state of the sensitizer dye into the conduction band of the nanocrystalline semiconductor. The presence of liquid electrolyte, usually an iodide/tri-iodide redox couple dissolved in an organic solvent is to regenerate the dye cation produced after electron transfer. Furthermore, the regeneration of iodide ions, which are oxidized in this reaction to tri-iodide, is achieved at counter electrode. To enhance the photo electrochemical behavior of DSSC, several key issues have been identified,

including a desired semiconductor oxide mesostructure, development of novel sensitizing dyes and electrolytes (both liquid and solid types), and employment of new alternative counter electrodes [4-7]. TiO_2 nanoparticles have been used as the photo electrode in DSSC because of its high surface area and allow the adsorption of a large number of dye molecules. These nanoparticles have been prepared by several synthetic routes in a variety of particle sizes, pore size distributions and crystallinities. These factors affect the electron transport and as a consequence, the charge recombination kinetics and the dark current of these cells [8].

Among other techniques to prepare TiO_2 thin films, sol−gel process has been widely practiced. It is a wet chemical route which involves the evolution of a system from a colloidal suspension (the "sol") into a solid/semi-solid (the "gel") phase. Upon the evolution, two important reactions namely *hydrolysis* and *condensation* are associated. This process was developed initially as a technique to prepare pure ceramic precursors and inorganic glasses at low temperatures. Owing to its versatility [9], nowadays sol−gel process has been intensively studied and practiced into applications to respond to the demand for advanced ceramics of high purity, well-controlled homogeneity, and properly tailored properties as well as various nanostructured materials [10]. On top the advantages offered, however, the sol−gel process has a major limitation, which is the low crystallinity in the resulting TiO_2 phase, as a consequence of the relatively low processing temperatures. In connection with this problem, Brinker and Hurd [11] and Langlet *et al.* [12] proposed that the largely amorphous nature of TiO_2 films could be due to the high functionality of titanium alkoxide favoring the fast development of a stiff Ti−O−Ti network, which in turn hinders the condensation and densification during drying. In this connection, further studies by Matsuda *et al*. [13] and Kotani *et al*. [14] suggested that structural changes of sol−gel films can be induced by the treatment in a high humidity environment at temperatures above 100 ^oC. Further investigation by Imai *et al*. [15] and Imai and Hirashima [16] confirmed that exposure of sol−gel derived TiO_2 films to water vapor induced rearrangement of Ti-O-Ti network leading to formation of anatase phase at relatively low temperature (180 ^oC). It is thus of interest to investigate whether an appropriate water vapor treatment can be applied and promote crystallization of the sol−gel derived TiO_2 nanoparticles in the present study. Moreover, the current works is aimed at finding the correlation between the TiO_2 nanostructure features, electronic characteristics and the performance of the resulting DSSC fabricated from the sol−gel derived TiO_2 nanoparticles and understanding the mechanism behind the phenomena from the point of materials science and technology. For this purpose, nanocrystalline TiO_2 was synthesized through a sol−gel technique with a variation in water to inorganic precursor or hydrolysis ratio (R_w) of 0.85, 2.00 and 3.50 upon sol preparation, followed with subsequent drying, conventional annealing and post-hydrothermal treatments to control the crystallinity of TiO_2 phase.

2. Experiment

In this work, TiO_2 nanoparticles were synthesized via a well-controlled sol−gel process where the titanium tetra-isopropoxide (TTIP, 98%, Acros) precursor was first mixed with ethanol (Et-OH, 95%, Merck) in a container and stirred for 30 minutes. A mixture of deionized water and hydrochloric acid (HCl, 36%, Merck) was then added under stirring condition into the transparent solution to promote hydrolysis. The TTIP concentration in the solution was fixed at 0.4 M with the ratio of water to TTIP (R_w) was varied as 0.85, 2.00 and 3.50 while the pH of all solution was kept consistent at around 1.30 for obtaining a stable-highly transparent solution. The solution was further stirred overnight and poured into a petri-dish to form thick films. The thick films were dried at room temperature for 1 week and 60 ^oC for 3 days. Respective TiO_2 powder samples were made by grinding them carefully in the mortar. These powder samples were subjected to conventional annealing in dry atmosphere at 150 ^oC for 24 hours and subsequent post-hydrothermal treatment with highly pressurized water vapor at 150 ^oC for 24 hours. For the post-hydrothermal treatment, a Teflon-lined stainless steel autoclave (Parr, Moline, IL) was used where a specially-designed stand was placed inside the autoclave in order to prevent the samples from direct contact with liquid water.

In order to examine the effect of various R_w on the size of the inorganic species upon hydrolysis and condensation reactions, particle size measurement was directly conducted on the resulting TiO_2 sols using Delsa^{TM} Nano Submicron dynamic light scattering. Further characterization on dried, conventionally annealed and post-hydrothermally treated TiO_2 nanoparticles was carried out with X-ray diffraction (XRD) measurementson Bruker AXSθ–2θ diffractometer using Cu K-α radiation (1.5406 Å) operated at 40 kV, 40 mA and with a step-size of 0.02^o and time/step of 20 seconds. The crystallite sizes of TiO_2 nanoparticles were estimated using Scherrer's equation [17]:

$$t = \frac{0.9\lambda}{B\cos\theta} \quad (1)$$

where t is the average crystallite size, λ is the X-ray wavelength, θ is the Bragg's angle and B is the line broadening, based on full-width at half maximum (FWHM) in radians. It should be noted, that for the sake of proper calculation, other aspects contributing to the broadening due to strain in the sample and instrumentation were considered [17,18].

The corresponding infrared spectra of TiO_2 samples were recorded at room temperature in the range of 4000−400 cm^{-1} using Bio-Rad FTIR model QS-300 spectrometer, which has a resolution of + 8 cm-1. Their diffuse reflectance spectra were obtained by using UV-Vis spectrophotometer (UV-1601, Shimadzu) at the wavelength range of 800−200 nm with a resolution of $\pm$ 0.3 nm. The band gap energy (E_g) of TiO_2 nanoparticles were estimated by analyzing the Kubelka Munk function on the measured reflectance spectra [19]. X-ray photoelectron spectroscopy (XPS) was acquired by using a VG Scientific ESCALAB MKII with concentric hemisphere analyzer operated in the constant energy mode. A pass energy of 50 eV was employed for the wide scan survey spectrum while 20 eV was used for high resolution core level scans. The exciting source was a Mg Kα operated at 150 W (10mA; 15kV) and the spectra were recorded using a 75° take off angle relative to the surface normal. All XPS core level spectra were fitted with XPSPEAK 4.1 program. The fitted XPS spectra were corrected for sample charging by applying a binding energy shift such that the hydrocarbon component of each C1s region was centered at 285 eV. The nanostructure of TiO_2 nanoparticles was examined finally by using a transmission electron microscope operating at 200 keV and with a resolution of 0.14 nm (JEOL -3010).

The route for DSSC fabrication in this work is adopted from the procedure reported in the reference [20]. The working photo electrode was made by using doctor blade (slip cast) technique to deposit a layer of TiO_2 slurries on conducting glass (ITO, Every Rich Entreprise Ltd, sheet resistance 15 Ω /$inch^2$). The slurries were prepared by thoroughly mixing 1 g of nanoparticle TiO_2 and/or ZnO powder with 2 ml distilled water, 5 drops of a non-ionic surfactant (Pluronic P123, BASF) and 2 drops acetylacetone (Sigma-Aldrich). The homogeneous slurries were further sheared over the glass substrates with a glass rod resulting in electrode area of 0.25 cm^2. The resulting layer was dried at room temperature for 30 minutes and further sintered at 450 °C for 35 minutes to remove the organic residues and to establish electrical contact between the TiO_2 nanoparticles. After being cooled to room temperature, the TiO_2 photo electrodes were immersed in sensitizing dye solution, which were made from red onion extract, for 24 hours. The photo electrodes were removed form dye solution, washed thoroughly with acetonirile and finally dried. At the same time, a counter electrode was made by carbonizing another ITO glass. The DSSC prototype was finally obtained by sandwiching the working and counter electrodes. The cell was completed by filling the mixture of KI and I_2 as electrolyte through a small prefabricated hole in the counter electrode. The electrolyte is spread in very thin gap between the electrodes. To prevent electrolyte evaporation, the cells were sealed with thermoplastic film. The DSSC testing was performed with a white-light source and the open circuit voltage (V_{oc}) was measured using a multi-tester.

3. Results and Discussion

The present work was first focused on investigating the effect of TiO_2 nanocrystallites size on the open circuit voltage (V_{oc}) of the DSSC. For this purpose, the semiconductor oxide layer in the device was made by mixing the commercial TiO_2 and ZnO powders, where ZnO acts as the matrix in the mixture. The TiO_2 incorporated into the oxide mixture was in the size of nano and micrometer. Owing to their scale, they were termed as TiO_2 nano and TiO_2 micro-*as received*, respectively. In order to confirm the phase and size of TiO_2 nanocrystallites, XRD was performed on both samples and the results are given in Fig. 1.

The diffraction peaks are clearly shown at 2θ of 25.35, 48.25, 38.45, 54.85 and 63.38° corresponding to (101), (200) (112), (211) and (204) crystal planes for anatase titania. It is well-known that the XRD peaks are related to the crystallites characteristics [17,18]. The broadening of X-ray diffraction in trace "a" as shown in the inset of Fig.1 strongly suggests the nanocrystalline nature of TiO_2 phase in sample TiO_2 nano. Scherrer's

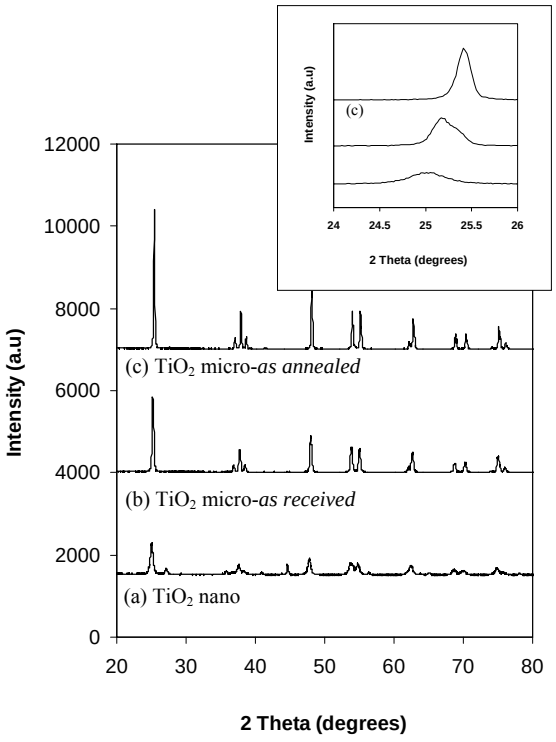

Fig.1. XRD Traces of the Samples: (a) TiO_2-Nano; (b) TiO_2 Micro-*as Received*; (c) TiO_2 Micro-*as Annealed* Inset is the Broadening of (101) Peak Shown by Samples a, b, and c Indicating the Different Sizes of TiO_2 Nanocrystallites

formula was employed to estimate the crystallite size of TiO_2 nano (trace "a) and TiO_2 micro-*as received* (trace "b") Note that an additional sample namely TiO_2 micro-*as annealed* was included in the test (trace "c). This sample was purposely subjected to annealing process at 600 ^oC for 24 hours and was used as a standard sample to exclude the broadening due to instrument effect throughout the use of Scherrer's formula. The calculations showed that the crystallite size of TiO_2 nano (trace "a) and TiO_2 micro-*as received* (trace "b") is 28 and 137 nm, respectively. The result confirmed the significant difference in particle size between TiO_2 nano and TiO_2 micro-*as received*.

Fig.2 shows the open circuit voltage (V_{oc}) of the DSSC as a function of TiO_2 addition into the ZnO matrix. It is obviously shown that an increase of TiO_2 micro (▨) from 7.77 up to 38.89 wt% affected the V_{oc} of DSSC adversely from 42.20 down to 4.93 mV. On the other hand, the addition of the same composition of TiO_2 nano (⬚) has provided a positive impact, *i.e.* an improvement in the V_{oc} of DSSC from 6.93 to 46.57 mV. It is highly possible that the increase of TiO_2 addition has decreased detrimentally the contact area between the semiconductor oxide and the sensitizing dye. However, this is not the case for TiO_2 nanoparticles addition since they have a very large surface area, providing a synergistic effect for the sensitizing dye to inject the electron to the semiconductor and thus better electron transfer for light-electricity conversion. The result demonstrated the use of TiO_2 as nanoparticles in the DSSC is more pronounced than the bulk-micro particles.

On the basis of the previous results, our further investigation is focused on the TiO_2 nanoparticles derived from sol−gel process with various hydrolysis ratio (R_w) and treatments. The main concern is to know whether the variation in the synthesis parameters affects the nanocrystallinity of TiO_2 and thus the performance of the resulting DSSC. Several characterizations were performed to confirm the difference in nanocrystallinity among the samples. Table 1 provides the result of dynamic light scattering of TiO_2 sol with different R_w. It is clearly demonstrated that with increasing the water content added to the inorganic precursor upon sol−gel process has increased the particle size significantly. However, it should be noted that the values are not the size of solid nanocrystalline TiO_2. Instead, they represent the size of Ti−OH and Ti−O−Ti species resulted from hydrolysis and condensation reactions which have formed clusters or particle-like networks among the random and entangled chains of inorganic molecules (Fig. 3).

Figure 4 provides the XRD traces of the resulting TiO_2 powders derived from the sol−gel process with various hydrolysis ratios after drying, conventional annealing and post-hydrothermal treatment. It is clear that all *as-dried* samples are still amorphous as indicated by a very broad hump in the 2θ range of 20−35^o in traces "a", "b" and "c". The crystallinity enhancement started to occur when all the samples were subjected to the conventional annealing, as represented by slightly increase in the intensity for the diffraction peaks at 2θ angles of 25−26, 38, 48, and 54^o in traces "d", "e" and "f". Moreover, such significant enhancement as demonstrated with further increase in the above mentioned peaks was apparently shown by the post-hydrothermally treated samples (traces "g", "h" and "i"). Among these samples, it is interesting to note that the most enhanced nanocrystallinity was achieved by TiO_2 derived from sol−gel process with R_w of 2.00 (trace "h"). To obtain a more quantitative analysis on the size of TiO_2 crystallites derived from sol−gel with various R_w at conventional annealing and post-hydrothermal conditions, crystallite size was calculated using Scherrer's formula and the results are summarized in Fig. 5. From this figure, it can

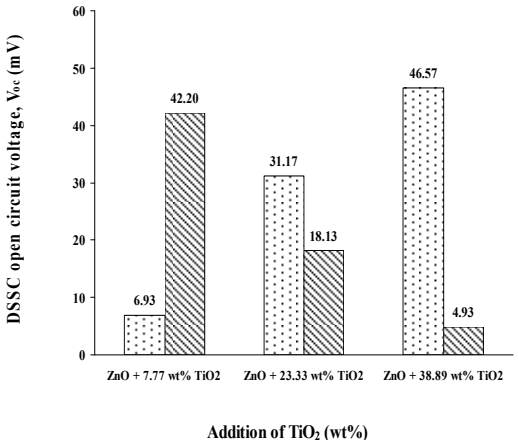

Fig. 2. The Result of V_{oc} Measurement of the DSSC as a Function of TiO_2 Addition Into the ZnO Matrix, TiO_2 nano (⬚), TiO_2 nano (⬚)

Table 1. The Result of Dynamic Light Scattering for the Particle Size in TiO_2 Sol with Various R_w

TiO_2 sol	Particle size (nm)
$R_w = 0.85$	1.90 ± 0.3
$R_w = 2.00$	3.70 ± 0.8
$R_w = 3.50$	17.90 ± 4.3

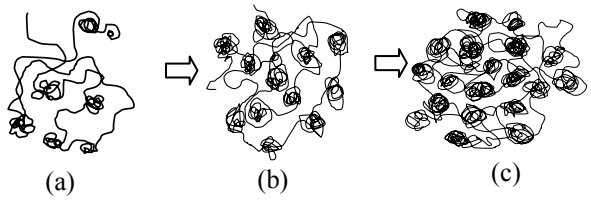

Fig. 3. The Growth of TiO_2 Nuclei in the Sol as a Result of Hydrolysis and Condensation Reactions with R_w of: (a) 0.85; (b) 2.00 and (c) 3.50

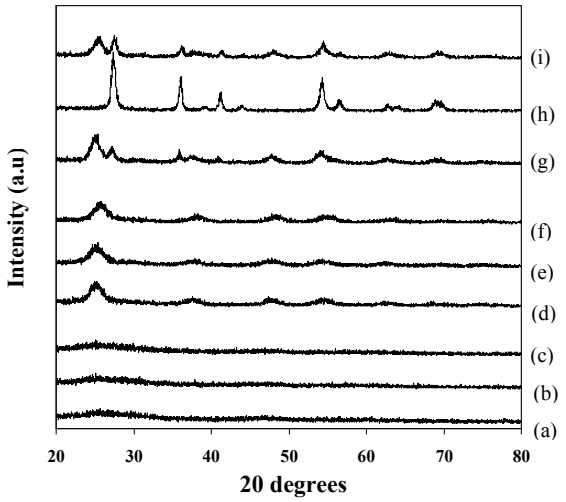

Fig. 4. XRD Traces of TiO_2 Derived from Sol−Gel Process with R_w of 0.85; 2.00 and 3.50 at Drying (Traces "a", "b" and "c"), Conventional Annealing (Traces "d", "e" and "f"), and Post-Hydrothermal (Traces "g", "h" and "i") Conditions, Respectively

be seen that with the increase of R_w from 0.85 to 2.00, the crystallite size of TiO_2 nanoparticles increased from 3.10 to 4.07 nm for annealed condition (▨), and from 4.84 12.46 nm for post-hydrothermal condition (⊡). However, a further R_w increase to 3.50 has resulted in a decrease in crystallite size down to 3.81 and 7.21 nm respectively, although these values are still higher than those shown by R_w of 0.85. It is also apparently demonstrated that the post-hydrothermally treated sample with R_w of 2.00 provides a much more pronounced nanocrystallinity enhancement as represented with a significant increase in the crystallite size up to 12.46 nm. In order to further understand the mechanism behind the results, further characterizations with FTIR, XPS and TEM were performed.

Figure 6 shows the result of FTIR spectroscopy, aimed at investigating the nanocrystallinity difference between the conventionally annealed and post-hydrothermally treated TiO_2 samples. It shows obviously the existence of broad absorption bands located at ~3400−3500 cm^{-1}, which is assigned to hydroxyl groups of Ti−OH [21]. In addition, there exists also an absorption band in the range of ~400−900 cm^{-1}, accounted for the stretching vibrations of Ti−O−Ti groups [22]. From the figure, it can be apparently demonstrated that the conventionally annealed sample (spectrum "a') provides a high intensity Ti−OH absorption band, but with a weak intensity in Ti−O−Ti absorption band. By contrast, a reverse phenomenon occurred for the post-hydrothermally treated sample (spectrum "b') where the intensity of Ti−OH absorption band decreased significantly, accompanied with an increase in the intensity of Ti−O−Ti absorption band.

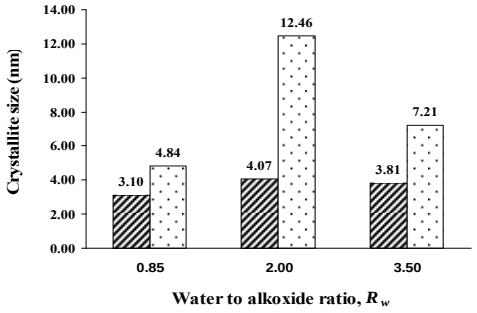

Fig. 5. The Estimated Crystallite Size of TiO_2 Samples Derived from Sol−Gel Process with R_w of 0.85, 2.00 and 3.50 at Conventional Annealing (▨) and Post-Hydrothermal Treatment Conditions (⊡)

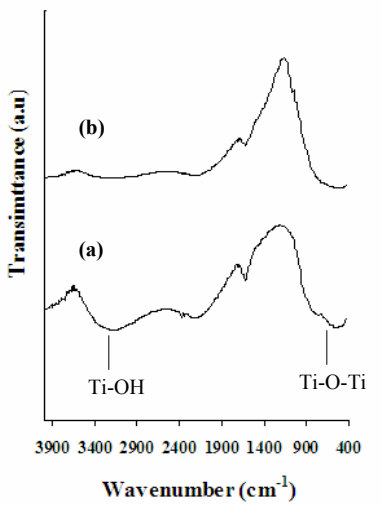

Fig. 6. FTIR Spectra of: (a) Conventionally Annealed and (b) Post-Hydrothermally Treated TiO_2 Nanoparticles Derived from Sol−Gel Process with R_w of 2.00

Figures 7a-b are the TEM images of TiO_2 nanoparticles derived from sol with R_w of 2.00 after conventional annealing and post-hydrothermal treatments, respectively. It can be seen that the post-hydrothermal treatment has significantly enhanced the crystallinity of TiO_2 phase, as indicated with clear lattice fringe (Fig. 7b) in comparison to the amorphous state of the conventionally annealed sample (Fig. 7a). The d-spacing of the lattice fringe is measured to be 0.352 $\pm$ 0.008 nm, which is in good agreement with the inter-plane spacing (*d*-value) of the (101) crystal plane in anatase TiO_2.

Figures 8a-b show the high resolution XPS spectra of O1s region for the conventionally annealed and post-hydrothermally treated TiO_2 samples, respectively. It can be seen both spectra demonstrate broad and asymmetric signals ranging from ~526 to 536 eV indicating the coexistence of different chemical environments on the TiO_2 nanoparticle surfaces. By

performing further analysis, each spectrum can be fitted into three peaks located at around 529.5-530, 531.5 ± 0.5, 533 ± 1 eV, attributed to oxygen in the metal oxide component (*i.e.* O^{2-} bound to Ti^{4+} in TiO_2 lattice), oxygen in the hydroxyl groups (–OH) or defective oxides, and physisorbed or chemisorbed molecular water, respectively [23]. The last two species are mainly associated with the TiO_2 surfaces. In the conventionally annealed sample (Fig. 4a), the estimated area percentage under the metal oxide peak was around 23.0%, which is considerably lower than that of the hydroxyl groups/ defective oxides (around 63.5%). This is in agreement with the fact that the TiO_2 phase in this sample is still largely amorphous, as has been shown by the XRD and TEM studies. Due to the strained characteristics of Ti–O–Ti bonds contained in the hydroxyl groups as well as non-stoichiometric nature of the defective oxides, a retardation towards formation of a well crystallized TiO_2 phase is therefore expected.

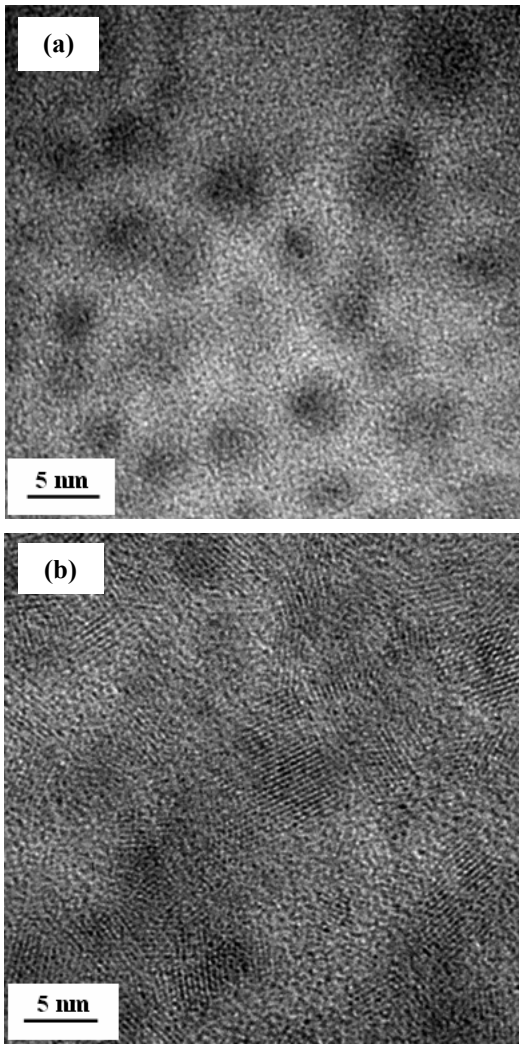

Fig. 7. HRTEM Images of: (a) Conventionally Annealed and (b) Post-Hydrothermally Treated TiO_2 Nanoparticles Derived from Sol–Gel Process with R_w of 2.00

On the other hand, when the post-hydrothermal treatment was applied, the percentage of metal oxide peak increases significantly up to around 49.0%, accompanied by a decrease in the hydroxyl-defective oxides peak down to around 42.3% (Fig. 8b). This confirmed the effectiveness of high pressure water vapor in converting the surface states of TiO_2 nanoparticles to less-defective ones, thus promoting the crystallinity. Similar results on the role of water vapor in removing the surface defects have been reported for bulk TiO_2 (110) surfaces by Wang *et al.* [24]. A reduction of chemisorbed water content from 13.5% to 8.7% was also observed, which is believed to be a consequence of the involvement of water molecules in the cleavage of the strained Ti–O–Ti bonds and their rearrangements into nanocrystalline TiO_2 phase.

By correlating the above FTIR, TEM and XPS analyses, it is obvious that the crystallinity enhancement of the sol–gel derived TiO_2 phase is represented with an increase in the intensity of Ti–O–Ti absorption band and a decrease in intensity of Ti–OH absorption band. The stretching vibration of Ti–O–Ti absorption band is

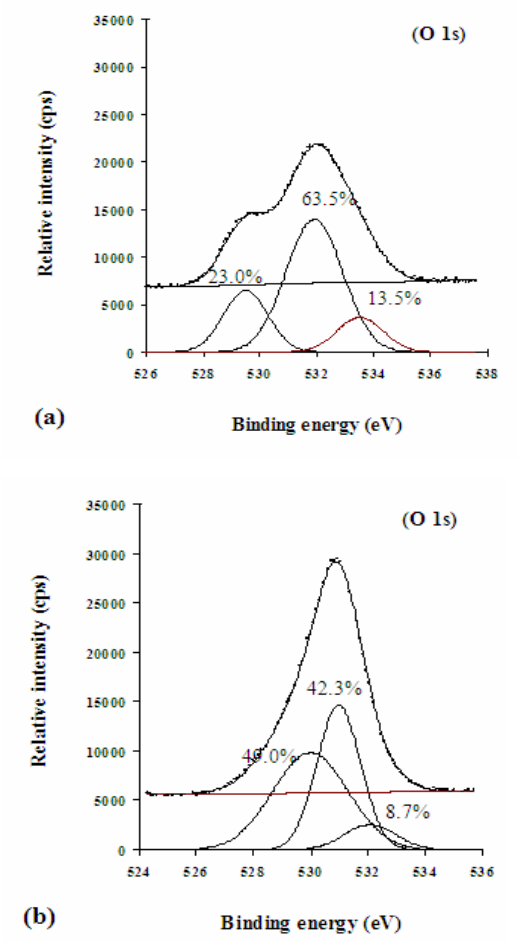

Fig. 8. XPS High Resolution O 1s Spectra of: (a) the Conventionally Annealed and (b) the Post-Hydrothermally Treated TiO_2 Nanoparticles

regarded as the characteristic peak for TiO_2 nanocrystalline [22]. The present study also has confirmed what has been proposed by Imai *et al*. [15] and Imai and Hirashima [16] that water vapor exposure in the post-hydrothermal treatment can successfully enhance the nanocrystallinity of TiO_2 phase as a result of cleavage mechanism of strained Ti−OH networks by high pressure water molecules to provide much more flexible Ti−O−Ti networks which can further densify to form nanocrystalline TiO_2. In connection with the previous results by Brinker and Hurd [11] and Langlet *et al.* [12], the current results show that the R_w of 2.00 is the optimum hydrolysis ratio that can lead to a proper number of Ti−OH species which function as flexible nuclei for the formation of TiO_2 nanocrystalline, both at annealed and post-hydrothermal conditions, while the R_w value of 3.50 caused an excessive formation of stiff Ti−OH networks which could not densify further to form TiO_2 nanocrystalline, although the cleavage mechanism has been applied on this sample during post-hydrothermal treatment.

Figure 9 compares the band gap energies (E_g) for TiO_2 samples under investigation resulted from Kubelka Munk analysis for the obtained UV-Vis reflectance spectra. Firstly, it is interesting to note that there is the same trend in the decrease of E_g shown by all the samples with different R_w, *i.e.* the highest E_g is given by the as-dried samples (▨), subsequently followed with the conventionally annealed (▩) and post-hydrothermally treated (▤) samples.

Secondly, for drying condition, the E_g decreased from 3.66 to 3.55 eV when the R_w increased from 0.85 to 2.00, but it increased back to 3.58 eV when R_w was further increased to 3.50. The same trend was also demonstrated by the other two conditions, *i.e*. 3.54, 3.49, 3.52 and 3.50, 3.48, 3.51 for conventionally and

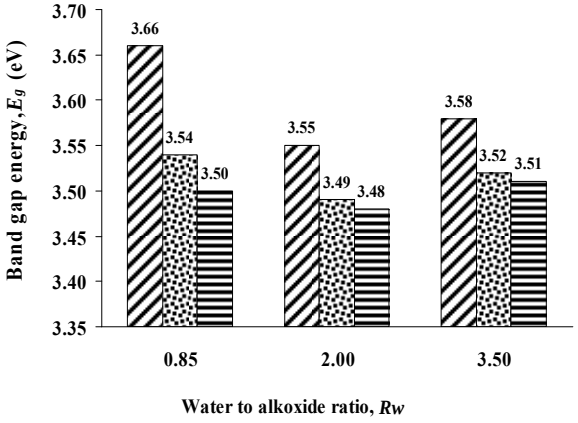

Fig. 9. The Result of Band Gap Energy (E_g) Estimation on the TiO_2 Samples Derived from Sol with R_w of 0.85, 2.00 and 3.50, Drying (▨), Conventional Annealing (▩), Post-hydrothermally Treatment (▤)

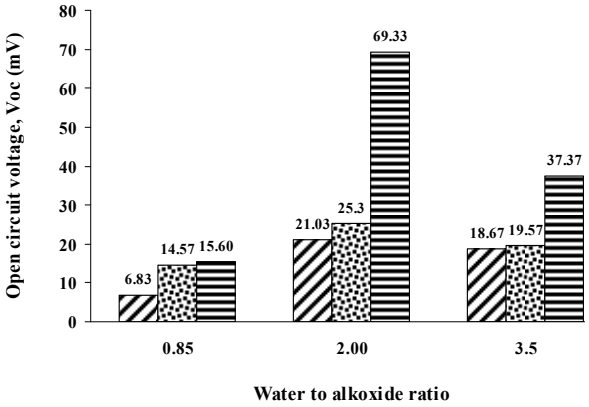

Fig. 10. The Result of DSSC Open Circuit (V_{oc}) Measurement of: Drying (▨), Conventional Annealing (▩), Post-hydrothermally Treatment (▤) TiO_2 Samples with R_w of 0.85, 2.00 and 3.50

post-hydrothermally treated samples, respectively. All of the treated samples show the lowest E_g when synthesized with R_w of 2.00. By correlating these results to the crystallite size analysis, it can be seen that the nanocrystallinity of TiO_2 nanoparticles affects their electronic properties. In this investigation, the post-hydrothermally treated sample with R_w of 2.00, which provided the biggest crystallites size, *i.e.* 12.46 nm, showed the lowest band gap energy, *i.e.* 3.48 eV.

The result of DSSC open circuit (V_{oc}) measurement is given in Fig. 10 for (a) as-dried (▨); (b) conventionally annealed (▩); and (c) post-hydrothermally treated (▤) TiO_2 samples on various R_w from 0.85 to 3.50. For all the samples of different treatments, the V_{oc} of DSSC device increased first when R_w was increased from 0.85 to 2.00, but it decreased at R_w of 3.50. This trend is in agreement with the crystallite size and in the consistent reverse direction with the E_g results. Therefore the R_w of 2.00 can be considered as the optimum hydrolysis ratio that can produce the more desired nanostructures characteristics, electronic properties (E_g) and DSSC $V_{oc.}$ The highest V_{oc} of 69.33 mV was obtained by the post-hydrothermally treated TiO_2 sample with crystallite size of 12.46 nm and E_g of 3.48 eV derived from the sol with R_w of 2.00.

The lowest Eg allows the electron injection from the sensitizing dye to TiO2 conduction band to be more effective, resulting in a much higher voltage in the DSSC. A low Eg also enables the excitation of electron from valence band to the conduction band at higher wavelength or less intense light absorption.

4. Conclusion

A systematic investigation has been conducted on semiconductor oxide TiO_2 derived from sol−gel process, aimed at understanding the mechanisms responsible for

the occurrence of the largely amorphous state in TiO_2 nanoparticles. The results confirmed that the low nanocrystallinity of TiO_2 is related to the fast development of stiff Ti−OH networks during hydrolysis and condensation upon sol−gel reaction. A post-hydrothermal treatment involving high-pressure water vapor has been successfully devised to enhance the nanocrystallinity of TiO_2 nanoparticles. The nano-crystallinity enhancement is resulted from the cleavage of stiff Ti−O−Ti bonds by water molecules, which effectively increases the number of flexible Ti-−OH groups and rearranges Ti−O−Ti bonds promoting crystallization of TiO_2. Moreover, the DSSC prototype has been successfully fabricated by using the resulting TiO_2 nanoparticles. It has been confirmed that nanosized oxide semiconductors can provide a better result for the DSSC voltage in comparison to the bulk ones. Further investigation on TiO_2 nanoparticles derived from the sol−gel process with R_w of 0.85, 2.00 and 3.50 has shown the correlation between the crystallite sizes, electronic band gap energy (E_g) and the open circuit voltage (V_{oc}) of the DSSC. In this study, the R_w of 2.00 has been found to be optimum for the sol preparation of TiO_2 precursor as it provided the most enhanced nanocrystallinity of 12.46 nm, the lowest band gap energy (E_g) of 3.48 eV and the highest DSSC open circuit voltage (V_{oc}) of 69.33 mV.

Acknowledgement

The authors would like to thank for the financial support from Hibah Riset Strategis Nasional Tahun 2009 of Ministry of Education-Republic of Indonesia through Directorate of Research and Community Services-University of Indonesia with contract no: 407CB/DRPM-UI/A/N1.4/2009. The research was also supported by Indonesian Toray Science Foundation (ITSF) Research Grant Year 2008.

References

[1] T. Priyambodo, Pembangkit listrik tenaga surya: memecah kebuntuan kebutuhan energi nasional dan dampak pencemaran lingkungan [Internet], 2007 [Diakses 21 May 2008]. Tersedia di: *URL:http://www.chem-is-try.org/?sect=artikel&ext=114*.
[2] M. Grätzel, Nature 414 (2001) 338.
[3] B.O'Reagan, M. Grätzel, Nature 353 (1991) 737.
[4] M. Grätzel, J. Photochem. Photobiol. A: Chem. 164 (2004) 3.
[5] G. Schlichthorl, S.Y. Huang, J. Sprague, A.J. Frank, J. Phys. Chem. B 101 (1997) 8141.
[6] N. Kopidakis, N.R. Neale, A.J. Frank, J. Phys. Chem. B 110 (2006) 12485.
[7] P. Wang, S.M. Zakeeruddin, M. Grätzel, Adv. Mat. 16 (2004) 1806.
[8] I.C. Flores, J.N. de Freitas, C. Longo, M.A. De Paoli, H. Winnischofer, A.F. Nogueira, J. Photochem. Photobiol. A: Chem. 189 (2007) 153.
[9] J.D. McKenzie, J. Non-Cryst. Solids 100 (1988) 162.
[10] K.N.P. Kumar, K. Keizer, A.J. Burgraaf, T. Okubo, H. Nagamoto, S. Morooka, Nature 358 (1992) 48.
[11] C.J. Brinker, A.J. Hurd, J. Phys. III France 4 (1994) 1231.
[12] M. Langlet, M. Burgos, C. Coutier, C. Jimenez, C. Morant, M. Manso, J. Sol−Gel. Sci. Technol. 22 (2001) 139.
[13] A. Matsuda, Y. Kotani, T. Kogure, M. Tatsumisago, T. Minami, J. Am. Ceram. Soc. 83 (2000) 229.
[14] Y. Kotani, A. Matsuda, T. Kogure, M. Tatsumisago, T. Minami, Chem. Mat. 13 (2001) 2144.
[15] H. Imai, H. Moromoto, A. Tominaga, H. Hirashima, J. Sol−Gel. Sci. Technol. 10 (1997) 45.
[16] H. Imai, H. Hirashima, J. Am. Ceram. Soc. 82 (1999) 2301.
[17] B.D. Cullity, Elements of X-ray Diffraction, 2nd ed., Addison-Wesley Reading, Massachusetts, 1978, p. 284.
[18] C. Suryanarayana, M.G. Norton, X-Ray Diffraction: A Practical Approach, Plenum Press, New York, 1998, p. 207.
[19] V. Kumar, S.K. Sharman, T.P. Sharma, V. Singh, Optic. Mat. 12 (1999) 115.
[20] I. Kartini, D. Menzies, D. Blake, J.C.D da Costa, P. Meredith, J.D. Riches, G.Q. Lu, J. Mat. Chem. 14 (2004) 2917.
[21] L.H. Lee, W.C. Chen, Chem. Mater. 13 (2001) 1137.
[22] S.X. Wang, M.T. Wang, Y. Lei, L.D. Zhang, J. Mater. Sci. Lett. 18 (1999) 2009.
[23] R. Sanjines, H. Tang, H. Berger, F. Gozzo, G. Margaritondo, F. Levy, J. App. Phys. 75/6 (1994) 2945.
[24] L.Q. Wang, D.R. Baer, M.H. Engelhard, A.N. Shulz, Surf. Sci. 344 (1995) 237.